Environmental Science & Technology

Article

pubs.acs.org/est

Capillary Pressure–Saturation Relations for Supercritical CO_2 and Brine in Limestone/Dolomite Sands: Implications for Geologic Carbon Sequestration in Carbonate Reservoirs

Shibo Wang and Tetsu K. Tokunaga*

Earth Sciences Division, Lawrence Berkeley National Laboratory, 1 Cyclotron Road, Berkeley, California 94720, United States

Supporting Information

ABSTRACT: In geologic carbon sequestration, capillary pressure (P_c)–saturation (S_w) relations are needed to predict reservoir processes. Capillarity and its hysteresis have been extensively studied in oil–water and gas–water systems, but few measurements have been reported for supercritical (sc) CO_2–water. Here, P_c–S_w relations of $scCO_2$ displacing brine (drainage), and brine rewetting (imbibition) were studied to understand CO_2 transport and trapping behavior under reservoir conditions. Hysteretic drainage and imbibition P_c–S_w curves were measured in limestone sands at 45 °C under elevated pressures (8.5 and 12.0 MPa) for $scCO_2$–brine, and in limestone and dolomite sands at 23 °C (0.1 MPa) for air–brine using a new computer programmed porous plate apparatus. $scCO_2$–brine drainage and imbibition curves shifted to lower P_c relative to predictions based on interfacial tension, and therefore deviated from capillary scaling predictions for hydrophilic interactions. Fitting universal scaled drainage and imbibition curves show that wettability alteration resulted from $scCO_2$ exposure over the course of months-long experiments. Residual trapping of the nonwetting phases was determined at $P_c = 0$ during imbibition. Amounts of trapped $scCO_2$ were significantly larger than for those for air, and increased with pressure (depth), initial $scCO_2$ saturation, and time. These results have important implications for $scCO_2$ distribution, trapping, and leakage potential.

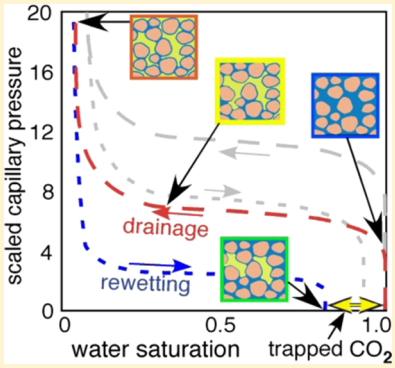

INTRODUCTION

Geologic carbon sequestration (GCS) in deep permeable saline aquifers is recognized as an effective technology to mitigate global warming caused by emission of anthropologic CO_2 from fossil fuel combustion.[1] Saline aquifers have the largest potential for storage of substantial amount of CO_2.[2] Captured CO_2 from anthropogenic sources is injected into porous deep subsurface formations (usually at depths greater than 800 m) as a supercritical (sc) fluid, followed by brine injection[3−5] or natural groundwater flow. Stratigraphic storage relies on integrity of the overlying seal (an intact caprock barrier to upward flow, usually shale). However, given the heterogeneity of the saline reservoirs and caprocks, stored CO_2 is under the risk of postinjection leakage, which would render GCS ineffective. Basic mechanisms controlling CO_2 storage in reservoirs and potential leakage through caprocks are incompletely understood.[6,7] At the pore scale, capillarity helps to immobilize CO_2. Understanding the fundamental relations between capillary pressure (pressure of the nonwetting CO_2 phase relative to brine, P_c), brine saturation (S_w), wettability (i.e., contact angle, θ), interfacial tension (IFT, γ), and pore structure is the basis for reliable prediction of the distribution, displacement and fate of CO_2 and brine. Therefore, measurements of P_c–S_w relations for $scCO_2$–brine in reservoir media are needed to mechanistically understand GCS processes.

During injection, the distribution of CO_2 and brine in the pore space varies with distances from the well, and is controlled by the drainage P_c–S_w relation of the reservoir. Likewise, in the postinjection stage, the pumping pressure is removed and brine tends to reoccupy pores. This competition between CO_2 and brine and their redistribution are described with the imbibition/rewetting P_c–S_w curves. The incomplete rewetting of reservoirs with resident brine allows retention of significant amounts of CO_2 in reservoirs by means of capillary/residual trapping, a major storage mechanism. Capillary trapping relies on the path- and history-dependent saturation characteristics to control distributions of multiphase fluid flow in pore spaces.[8−10] P_c–S_w behavior and capillary trapping capacity are difficult to predict due to complex dependence on fluid properties, porosity, pore geometry and tortuosity, pore size distribution, wettability, reservoir mineralogy, geochemistry, and surface chemistry. These factors all influence pore fluid dynamics such as Haines jumps (episodic displacements of menisci through irregular pores), thin film flow, and snap-off (disconnection of the nonwetting phase when passing pore constrictions), and hence affect capillary trapping.[11−13]

The determination of CO_2–brine P_c–S_w relations requires measurements of drainage and imbibition of the wetting phase (WP) fluid. Drainage of brine (the WP) by the invading $scCO_2$

Received: February 13, 2015
Revised: May 1, 2015
Accepted: May 6, 2015
Published: May 6, 2015

DOI: 10.1021/acs.est.5b00826
Environ. Sci. Technol. 2015, 49, 7208−7217

(the nonwetting phase, NWP) requires a P_c large enough to displace menisci through pore throats, and reaches the process-specific irreducible brine saturation, $S_{w,ir}$. When brine imbibes back into the pore space, a lower P_c is required for refilling pore bodies, resulting in P_c-S_w hysteresis. This capillarity-driven movement is opposed by viscous resistance and snap-off of NWP ganglia, leaving some $scCO_2$ retained in the pore network that constitutes the residual $scCO_2$ saturation, $S_{nw,r}$.

NWP (e.g., air, oil, and gas) trapping in consolidated cores[14−21] and unconsolidated sand packs[5,22−24] have been extensively studied. The residual trapped NWP saturation $S_{nw,r}$ is found to depend on pore network characteristics (e.g., porosity φ, pore size distribution, relative permeability κ_r) and initial NWP saturation, $S_{nw,i}$. Empirical relations have been developed to correlate $S_{nw,r}$ with $S_{w,ir}$, $S_{nw,i}$, κ_r, and φ. Land's model[16,25] has been demonstrated to reliably predict $S_{nw,r}$ in consolidated porous media and a doubly linear fit by Aissaoui[26] provides a generally reliable prediction of $S_{nw,r}$ for unconsolidated sandpacks.

P_c-S_w measurements in core analysis are routine, often by mercury injection, porous plate or centrifuge methods. However, very few direct measurements of P_c-S_w relations are available with $scCO_2$−brine fluid pairs under elevated temperature and pressure (ETP) representative of in situ reservoir conditions.[27−32] Most of the published data only covered drainage. However, evaluation of the complete drainage−imbibition loop is required to determine $S_{nw,r}$. To our knowledge, only the studies by Plug and Bruining[27] and Tokunaga et al.[32] determined S_{nwr,CO_2} during imbibition. Plug and Bruining[27] measured drainage and imbibition relations in quartz sand packs of different grain sizes, using several fluids including CO_2, using the porous plate method under room temperature and pressure (RTP), and ETP (26−28 °C, 0.8 MPa; 27 and 40 °C, 8.5 MPa). Typical drainage and imbibition behaviors were captured but instability/fluctuations in P_c and deviations of P_c from predicted values were noticed. The shift to lower-magnitude and even negative P_c was interpreted as wettability alteration. Tokunaga et al.[32] used the porous plate method to measure drainage and imbibition P_c-S_w relations on quartz sand packs ($250 < D_{50} < 355$ μm) under RTP (23 °C, 0.1 MPa, air−brine) and ETP (45 °C, 8.5 and 12 MPa, $scCO_2$−brine). The use of homogeneous sands facilitated comparisons with previous studies and application of capillary scaling. The P_c-S_w relations for $scCO_2$−brine deviated from the expected universal scaling curves for hydrophilic sands, indicating pronounced wettability alteration.

Capillary scaling has long been used to predict equilibrium and flow of immiscible fluids.[8,33−37] The scaled capillary pressure, Π_c (eq 1) can be defined by assigning either a characteristic pore or grain size in a porous medium to a capillary length scale λ:

$$\Pi_c = \frac{\lambda P_c}{\gamma} \tag{1}$$

to predict universal drainage and rewetting Π_c-S_w relations that are descriptive of geometrically equivalent porous media (sharing common φ and θ).[8,27,32,35−40] A less rigorous but more general scaling of P_c can be obtained through including a scaling factor w ($0 \leqslant w \leqslant 1$, sometimes assumed to be equivalent to $\cos\theta$) which qualitatively represents wettability.[41,42]

$$\frac{\Pi_c}{w} = \frac{\lambda P_c}{w\gamma} \tag{2}$$

Including wettability information in capillary scaling is complicated by surface roughness, contact angle hysteresis, and varying wetting properties of different surfaces within porous media. P_c-S_w measurements in homogeneous sand enable comparisons to an existing large body of literature with air and oil as the NWP.[33,36,37] For these reasons, this work is restricted to comparing P_c-S_w relations between air−brine and $scCO_2$−brine fluid pairs in homogeneous sand packs.

It has been assumed that capillary trapping of $scCO_2$ can be predicted based on the measured behavior of air, oil, and gas,[4,5,45,46] and several recent studies have provided experimental support for this expectation, both macroscopically[29−31,43,44] and at the pore scale.[47−49] However, some measurements under GCS relevant conditions have yielded contrary results.[13,27,32,45] For sandpacks, 25% (40 °C, 8.5 MPa[27]) and 8−32% S_{nwr,CO_2} (45 °C, 8.5 and 12.0 MPa[32]) were reported, respectively. On a partially brine-saturated (14−27% S_{nwi,CO_2}) Berea sandstone core plug, 7−17% S_{nwr,CO_2} (50 °C, 4.14 MPa) were obtained.[13] This latter result is inconsistent with the expectation that consolidated porous media generally retain more NWP due to greater pore heterogeneity and mixed wetting conditions.[29]

Understanding residual trapping of $scCO_2$ (quantified by S_{nwr,CO_2}) after water influx back into reservoir media is an important goal of P_c-S_w measurements. Given the few direct measurements performed under reservoir conditions, and uncertainties in capillary trapping and wettability mechanisms as described earlier, there remains an urgent need for measuring P_c-S_w with $scCO_2$ in porous media. Although P_c-S_w relations in quartz sands, and measurements of S_{nwr,CO_2} have been reported,[27,32] no investigations into carbonate-dominant sands have been performed to our knowledge.

This study was designed to gain understanding on equilibrium capillary and trapping behavior of $scCO_2$−brine in limestone/dolomite sands under reservoir conditions. Novel contributions include first-of-a-kind data of repeatedly measured brine drainage and imbibition curves to examine the time-dependent nature of these relations and consequent wettability hysteresis in limestone sand under air−brine at RTP (dolomite sand as well) and $scCO_2$−brine at ETP conditions over time scales of several months. The two elevated pressure conditions correspond to reservoir depths of 0.85 and 1.2 km, respectively, permitting evaluation of effects of injection depth on P_c-S_w relations. The semipermeable porous plate methodology was used with our custom-built high-pressure P_c-S_w regulator/meter mounted onto a programmed linear actuator system. The P_c-S_w data were then analyzed using capillary scaling to help identify changes in wettability and to determine residual $scCO_2$ trapping.

MATERIALS AND METHODS

Porous Media. Well-sorted limestone and dolomite sands (250−355 μm, Specialty Minerals Inc.) were used because they have well-defined pore size and structure. The sands were only cleaned with deionized (DI) water rinsing several times to best preserve their surface properties. Small amounts of pore lining materials and trace amounts of natural organics may be present, as they are in nature, and may influence interfacial phenomena.

DOI: 10.1021/acs.est.5b00826
Environ. Sci. Technol. 2015, 49, 7208−7217

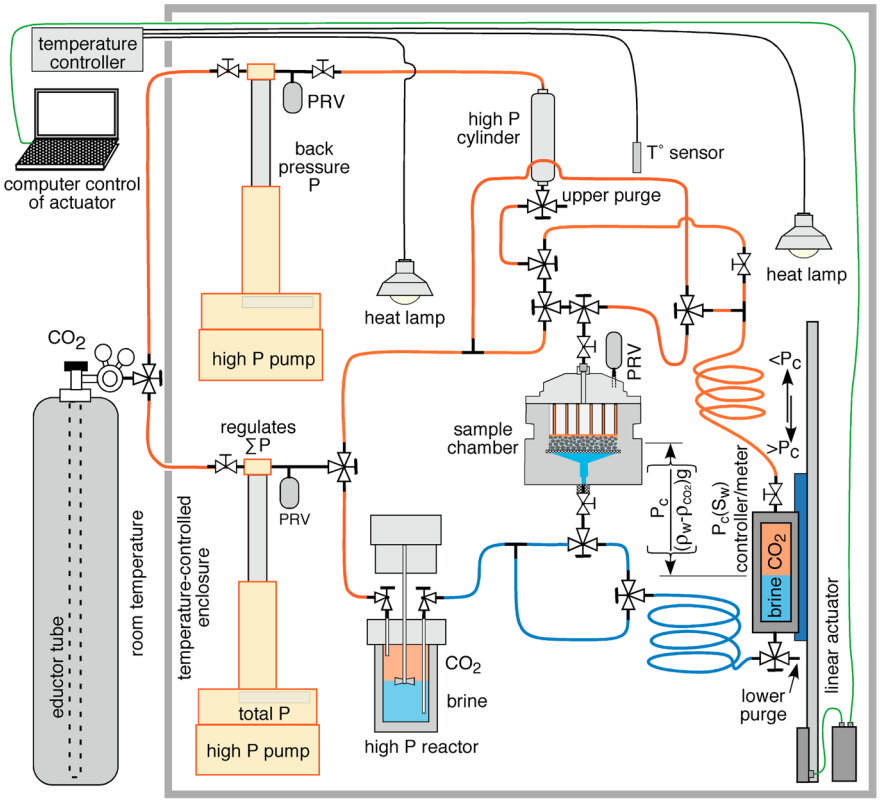

Figure 1. ETP $scCO_2$ experimental system. The sample's P_c is controlled by its elevation relative to the $scCO_2$–brine interface in the high-pressure P_c–S_w controller/meter, which moved vertically under control via a precise computer programmed linear actuator. Pressure relief valves (PRV) are located at the pump and on the sample chamber cap. Red lines = $scCO_2$, blue lines = brine.

More details on the samples are provided in the Supporting Information (SI Figures S1 and S2, Table S1).

Fluids. Three fluid pairs, i.e., air–brine, 8.5 MPa $scCO_2$–brine and 12.0 MPa $scCO_2$–brine were investigated. A synthetic brine solution of moderately high salinity (1.0 M NaCl, ACS grade, VWR Corp.) was used as the WP in all the experiments. The brine solution was prepared freshly before every measurement. The experiments with air were carried out under RTP (0.1 MPa, 23.0 ± 0.5 °C) and those with CO_2 were conducted under ETP reservoir conditions (8.5 and 12.0 MPa, 45.0±1 °C). Fluid properties under the experimental conditions are summarized in SI Table S2.

Experimental System and Procedures. The "hanging water column" method with semipermeable porous plate was the methodological basis for this study.[8,32] The porous plate enabled flow of brine and exclusion of $scCO_2$ between the sandpack and underlying fluid cavity, allowing establishment of finite P_c in the sand. Here, this method was applied to obtain hydrostatic equilibrium WP drainage and imbibition information using a semiautomated multistep outflow–inflow apparatus under reservoir conditions. The earlier design of the high-pressure sample chamber for $scCO_2$ experiments[32] was further improved as described in the SI. It should be noted that the time-consuming ETP P_c–S_w experiments were only conducted on limestone sand and not on dolomite sand because the RTP P_c–S_w experiments conducted with air–brine on both minerals indicated indiscernible differences (SI Figure S5). A description of the RTP experiments is presented in the SI.

In the $scCO_2$ experimental system (Figure 1), the P_c–S_w controller/meter simply consisted of a high-pressure sight glass reservoir (30 mL capacity, 34.5 MPa rated, Series T-40, Jerguson) with a volumetric graduation superimposed on its sapphire window. The sight glass vessel served a dual purpose to regulate P_c and be a reservoir for quantifying outflow/inflow brine from/into the sandpack. The sight glass was mounted on a computer programmed digital linear actuator (0.1 mm height resolution, ER50, Parker Hannifin Corp.). P_c was accurately controlled by adjusting the elevation of the $scCO_2$–brine interface in the sight glass relative to that of the sample center (horizontal midplane) via the linear actuator. The sight glass' upper and lower ports were connected to the syringe pump (500D HP, Teledyne Isco Corp.) and the sample chamber's upper port (brine-saturated $scCO_2$), and the sample chamber's lower port ($scCO_2$-saturated brine), respectively. The upper ports of the sample chamber were also connected with a high-pressure cylinder (316 stainless steel, 150 mL, 34.5 MPa rated, Swagelok Co.) for the purpose of initial flushing of sample column and sight glass with $scCO_2$-saturated brine. The cylinder was back-pressured at a slightly lower level (0.01 to 0.05 MPa) than the system's pressure by a secondary syringe pump of the same type. Several stainless steel high-pressure ball and needle valves (17.2 MPa rated, Swagelok) were placed in the loop to control fluid flow. The operation of the ETP experiment is described in the SI.

Constant temperature control was important during the months-long P_c–S_w experiments. Prior to the experiments, the main components of the system were connected via stainless steel and polyetheretherketone (PEEK) tubing and contained within a thermally insulated, temperature-regulated enclosure at 45.0±1 °C (Figure 1). The system's temperature was

DOI: 10.1021/acs.est.5b00826
Environ. Sci. Technol. 2015, 49, 7208–7217

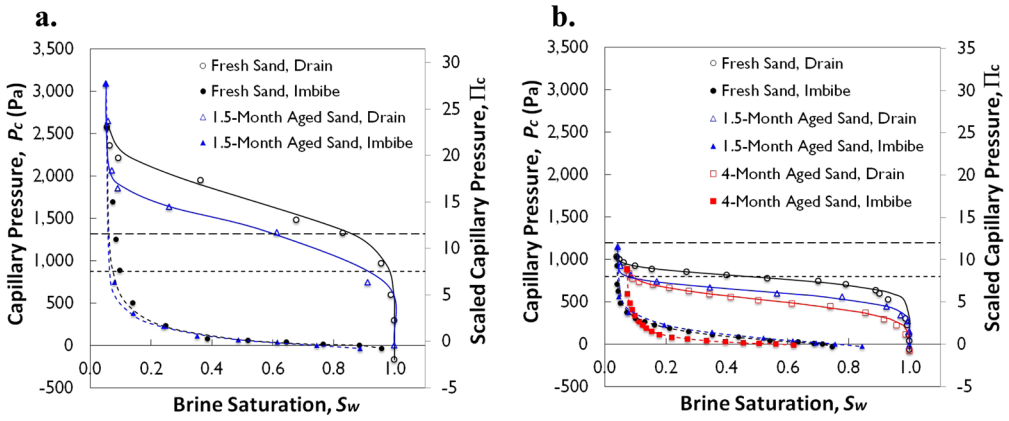

Figure 2. P_c−S_w relations during drainage and imbibition in limestone sand with $scCO_2$ at (a) 8.5 and (b) 12.0 MPa, 45 °C. The experiments involved two to three successive drainage-imbibition cycles with no waiting time between cycles. The sandpack was saturated with $scCO_2$ saturated brine (i.e., $S_{w,i}$ = 1.0) before every replicate cycle. Capillary-scaled Π_c dependence on brine saturation was also presented with universal scaling inflections (straight dash lines) included for comparison. Values of λ and γ used in capillary scaling are listed in SI Table S2. The data were fit with the van Genuchten model (equ 3),[52] with fitting parameters presented in SI Table S3.

maintained by four 250 W infrared halogen heating lamps which were distributed within the thermal enclosure.

This closed loop design allows control of P_c by setting the level of the $scCO_2$−brine interface in the sight glass window at the desired height below or above the sample. This configuration circumvented the instabilities and the difficulty of regulating P_c using separate pressure controllers for the two fluid phases. P_c and S_w can be controlled to very fine resolution ($\leqslant$10 Pa and 0.03, respectively), while maintaining the total pressure at any selected value safely containable by the system.[50,51] Because this method relies on adjusting elevations of the reservoir relative to the sample, the practical maximum height is about 1.5 m, which was adequate for conditions in this work.

Two and three successive replicate drainage-imbibition cycles were run at 8.5 and 12.0 MPa, respectively. Both 8.5 and 12.0 MPa experiments started with fresh limestone sands. Within the drainage cycle, the high-pressure P_c−S_w controller/meter was moved downward via the linear actuator to set the $scCO_2$−brine meniscus in the sight glass at a lower elevation (typically by 10 mm) to begin equilibration at a new P_c. Similar stepwise changes were imposed in order to progressively drain brine from the sandpack, until further brine removal with increased P_c became negligible, defining the experimental $S_{w,ir}$. At each step, the elevation of the meniscus inside the sight glass was recorded and the outflow volume of brine was quantified. The imbibition procedure followed, with the high-pressure P_c−S_w controller/meter sequentially raised until the system was returned to P_c = 0. It should be noted that full brine saturation was not achieved when P_c = 0 was reached during rewetting cycles due to residual trapping. The S_{nwr,CO_2} information was thus obtained from the total volume difference between drained and imbibed brine. Time intervals of 1 to 2 days (experimentally determined) between equilibration steps were used to ensure close approach to hydrostatic equilibration. A secondary (and tertiary for 12.0 MPa) drainage-imbibition cycle followed the primary one. In order to start with full brine saturation, the flushing procedures were repeated prior to the replicate runs. In the separate $S_{nw,r}$ vs $S_{nw,i}$ experiments, larger equilibration steps were used (details in the SI).

RESULTS AND DISCUSSION

P_c−S_w Relations. Experimental results are presented with P_c as the dependent variable in terms of $P_c(S_w)$ and $P_c(\Theta)$ where Θ (i.e., V_w/V_b, = φS_w) is the volumetric brine content. The drainage and imbibition data are presented in unscaled and scaled forms, where scaling is done initially with grain size, λ and IFT, γ as $\Pi_c(S_w)$ and $\Pi_c(\Theta)$, and then with λ, γ, and w as $\Pi_c(S_w)/w$ and $\Pi_c(\Theta)/w$. In SI Figure S5 and Figure 2, P_c and Π_c values are plotted on the primary and secondary vertical axes, respectively. Experimental data are shown as discrete data points, and the continuous curves are fits to the van Genuchten model (eq 3):

$$\Theta(P_c) = \Theta_r + (\Theta_s - \Theta_r)\left[\frac{1}{1 + (\alpha P_c)^n}\right]^m \quad (3)$$

where Θ_s and Θ_r are end point brine contents (highest and lowest values obtained in a given drainage or imbibition run), and α, m, and n are fitting parameters.[52] Θ_s and Θ_r are calculated based on the corresponding measured brine saturation values S_s and S_r by multiplying the porosity (0.38 here). The fitted parameters are listed in SI Table S3.

P_c dependence on brine (WP) saturation during drainage and imbibition for air−brine at RTP in the limestone and dolomite sands is presented in SI Figure S5. The data show reproducible trends between the duplicate runs, and insignificant differences between the P_c−S_w behaviors of limestone and dolomite sands. This highly consistent behavior supports investigation of limestone sand under ETP conditions to represent the common behavior shared among the carbonate sands. All drainage runs started at complete brine saturation ($S_{w,i}$ = 1.0), and reached $S_{w,ir}$ of 0.04 to 0.06 ($\Theta_{w,ir}$ from 0.015 to 0.021) at the end of drainage. For imbibition curves, nearly full brine saturation was obtained as the P_c was brought back to zero. The very low capillary trapping of air ($S_{nw,r}$ of 0.04 to 0.06 ($\Theta_{nw,r}$ from 0.014 to 0.021)) is typical of behavior reported for wetting fluids in homogeneous sands.[4,37]

The measured P_c−S_w relations permitted quantitative comparisons with capillary scaling predictions. Π_c−S_w curves are presented with the measured/unscaled ones on the same plots. Π_c values are calculated with γ (SI Table S2) and λ (λ = 302 μm, median of the 250 to 355 μm particle size interval) to

DOI: 10.1021/acs.est.5b00826
Environ. Sci. Technol. 2015, 49, 7208−7217

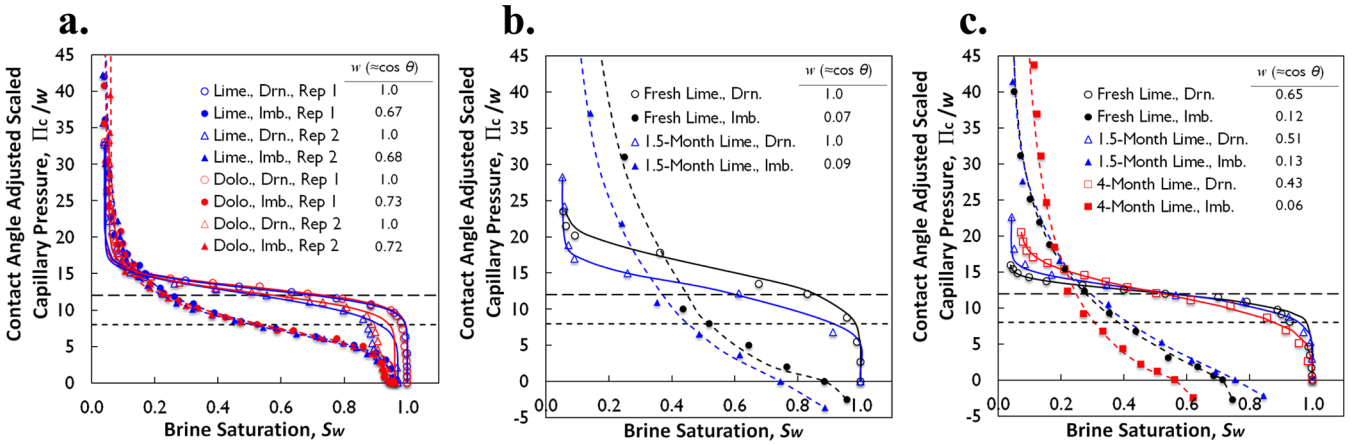

Figure 3. Fitting λ, γ, and w scaled capillary pressure Π_c/w through the characteristic inflection points by adjusting w for drainage and imbibition curves in limestone sand. Assumed w values (drainage/imbibition) for air-brine at (a) RTP and $scCO_2$–brine at (b) 8.5 and (c) 12.0 MPa, 45 °C are 1.0/0.67–0.73, 1.0/0.07–0.09, and 0.43–0.65/0.06–0.13, respectively. The fitted advancing and receding θ values and scaling inflections are summarized in SI Table S4. "Lime." = Limestone, "Dolo." = Dolomite, "Drn." = Drainage, "Imb." = Imbibition, and "Rep" = Replicate.

evaluate if the major inflections in drainage and imbibition curves can be predicted by these factors alone. For homogeneous, hydrophilic sands, Π_c–S_w curves have inflection values of ~12 for drainage and ~8 for imbibition curves (straight dash lines in SI Figure 5, Figure 2 and 3), respectively.[8,40] The scaled air–brine drainage Π_c–S_w curves agree very well with predicted Π_c inflection point for homogeneous sands, while the scaled imbibition curves have Π_c inflections lower than predicted (~6 instead of 8), indicative of slightly higher advancing contact angles (SI Table S4). The capillary entry pressure, $P_{c,entry}$, ranges from 2000 to 2500 Pa.

Measured drainage and imbibition P_c–S_w and scaled Π_c–S_w relations in limestone sand with $scCO_2$ at 8.5 and 12.0 MPa, 45 °C are shown in Figure 2. Two successive drainage-imbibition cycles were conducted at 8.5 MPa and three successive cycles were performed at 12.0 MPa to better investigate the exposure time effect of $scCO_2$ over 4 to 6 months. Single drainage or imbibition curve took 3 to 4 weeks, similar to the work by Bull et al.[53] Data reproducibility was fairly good for imbibition but less for drainage. $S_{w,ir}$ of 0.05 to 0.06 ($\Theta_{w,ir}$ from 0.020 to 0.021) and 0.04 to 0.07 ($\Theta_{w,ir}$ from 0.015 to 0.028) were obtained at the end of drainage runs at 8.5 and 12.0 MPa, respectively. $S_{nw,r}$ ranged from 0.11 to 0.25 ($\Theta_{nw,r}$ from 0.043 to 0.097) at 8.5 MPa and from 0.25 to 0.44 ($\Theta_{nw,r}$ from 0.093 to 0.167) at 12.0 MPa, which are comparable to previously reported values.[27,32,S4]

Comparisons among the repeated drainage-imbibition cycles for $scCO_2$–brine in limestone sand showed time-dependence, especially for drainage, where curves progressively shifted toward lower P_c. In general, $scCO_2$–brine drainage and imbibition occurred at significantly lower P_c than predicted. Scaling with λ and γ only significantly deviated from the universal inflection characteristic values (Π_c inflections ranging from 5.2 to 15.1 for drainage and from 0.5 to 1.1 for imbibition at intermediate S_w levels), as shown in SI Table S4. These results are important because S_w levels measured in field tests are mostly low to intermediate.[55] The data also show a significant swing of $P_{c,entry}$, ranging from 700 to 1000 Pa for 8.5 MPa and 200 to 600 Pa for 12.0 MPa. The small pressure-dependent differences in γ cannot explain the obvious difference between the 8.5 and 12.0 MPa P_c–S_w results.

Considering the P_c–S_w results of air–brine, 8.5 MPa $scCO_2$–brine and 12.0 MPa $scCO_2$–brine together (SI Figure S5 and Figure 2), the degree of hysteresis is governed by pore size distribution, wettability, viscosity ratio, and density difference.

The deviation of scaled curves based only on λ and γ from their characteristic inflection values implies that wettability of limestone sand altered toward more CO_2 wetting (i.e., increased contact angles). The scaling matches with measured data can be improved after adjustments for wettability are incorporated. As mentioned earlier, approximate scaling of wettability was performed through division of Π_c by w ($\Pi_c/w = \lambda P_c/w\gamma$). The advancing and receding contact angles (the upper and lower bounds of wettability with the equilibrium/static contact angle lying in between) during the drainage and imbibition experiments can be inferred by adjusting w values to fit the γ and w scaled curves through the universal scaling inflections. Assuming w (drainage/imbibition) to be 1.0/0.67–0.73, 1.0/0.07–0.09, and 0.43–0.65/0.06–0.13 provides satisfactory matching of our results with the inflection points at RTP, 8.5 and 12.0 MPa, respectively, as shown in Figure 3 and SI Table S4. The w values are numerically identical to $\cos\theta$, yet do not invoke scaling with θ. Thus, they are qualitative indicators of deviation from normal wetting, but do not quantitatively represent $\cos\theta$ values in pores (recalling the observation that water-wet contact angles inside the pore space of complex porous media tend to average around 45°).[41,42] Here, significant wettability hysteresis (difference between advancing and receding contact angles) is inferred from the Π_c/w data. Consistent with data in literature on dynamic contact angle,[56,57] water advancing (CO_2 receding) θ values obtained in the imbibition events are greater than those water receding (CO_2 advancing) θ values in the drainage events, with limestone being intermediate-wetting during imbibition for the $scCO_2$–brine cases. It should be noted again that the sands used in the experiments were only cleaned with DI water to retain their natural properties. The results were different from the generally water-wetting behavior of calcite measured on pristine and smooth mineral surfaces.[58–60] Given the significant surface roughness, the possible existence of pore lining minerals, and trace amounts of natural impurities and organics, more pronounced wettability alteration/hysteresis could have resulted from occasional contact line pinning and CO_2

DOI: 10.1021/acs.est.5b00826
Environ. Sci. Technol. 2015, 49, 7208–7217

adhesion onto carbonate species.[56,59] Direct pore-scale measurements of in situ contact angles for $scCO_2$–water have been obtained using micro-X-ray computed tomography (micro-XCT) and micromodel devices.[47−49,51] Micro-XCT of CO_2–brine in limestone yielded $\theta = 45° \pm 6°$.[49]

The comparison of P_c–S_w relations in limestone sand with those in quartz sand from our previous study[32] under the same experimental conditions was also made (SI Figure S6). P_c curves of limestone sand deviate more significantly from the universal scaling inflections than quartz sand. $S_{w,ir}$ values are similar, while $S_{nw,r}$ values in limestone sand are slightly larger than in quartz sand. Greater P_c hysteresis was observed in limestone sand than in quartz sand, and more pronounced wettability hysteresis occurred in limestone. This can be explained with the more favorable affinity at the molecular level between CO_2 and the carbonate species compared to SiO_2 in the carbonated brine environment and the likely occurrence of contact line pinning and CO_2 adhesion.[56,61]

Residual NWP Saturation. Quantifying residual trapping of NWP, $S_{nw,r}$ (=1−$S_{w,r}$, departure from complete brine saturation) at P_c = 0 at RTP and ETP was facilitated by accurate P_c control and S_w measurements in our experimental system. The determination of $S_{nw,r}$ at P_c = 0 instead of at the asymptotic limit of the saturation as P_c is increasingly negative best simulates the reservoir processes in the postinjection stage of CO_2 storage where spontaneous imbibition (instead of forced imbibition) mainly drives the brine to reoccupy the pore space and entrap CO_2. $S_{nw,r}$ and the capillary trapping capacity,[45] C_{trap} (=$\varphi S_{nw,r}$), i.e., volumetric fractions of trapped NWP relative to bulk sandpack volume were obtained for each air–brine, 8.5 MPa $scCO_2$–brine and 12.0 MPa $scCO_2$–brine experiment, as shown in Figures 4 and 5. The repeatability of $S_{nw,r}$ is fairly good, with the greatest amounts of NWP entrapment at 12.0 MPa. $scCO_2$ results collectively indicate that

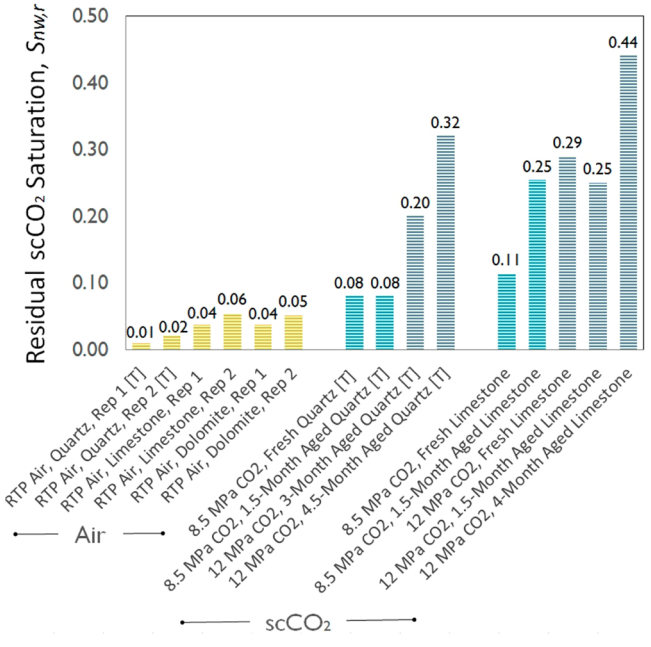

Figure 4. Measured residual NWP saturations, $S_{nw,r}$ obtained in limestone sand upon imbibition back to P_c = 0 for air–brine, 8.5 MPa $scCO_2$–brine and 12.0 MPa $scCO_2$–brine. Results in quartz sand under the same experimental conditions from previous study[32] are included for comparison (denoted as [T]). "Rep" = Replicate.

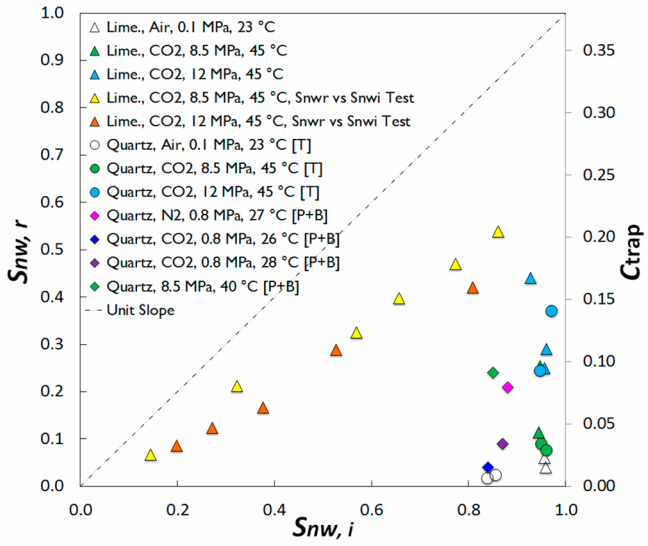

Figure 5. Residual NWP saturations, $S_{nw,r}$ and calculated capillary trapping capacity of NWP, C_{trap} (=$\varphi S_{nw,r}$), as a function of initial NWP saturations $S_{nw,i}$. Results in quartz sand under the same/similar experimental conditions from previous studies[27,32] are included for comparison (denoted as [P+B] and [T]). It should be noted that CO_2 dissolution was not excluded in the [P+B] data. "Lime." = Limestone.

capillary trapping of $scCO_2$ is much greater than that of air in carbonate sand, consistent with the results in previous studies on quartz sand.[27,32] Moreover, the amount of retained $scCO_2$ increases with increased pressure (reservoir depth), consistent with the previous experimental studies on quartz sands,[32] on carbonate reservoir core,[54] as well as modeling at the basin scale.[62] The porous medium properties (e.g., porosity, pore structure, and degree of compaction) and IFT are well constrained in our experiments, while capillary trapping significantly changed, showing that fluid properties (e.g., density difference, viscosity ratio) and fluid–fluid–solid interactions (e.g., wettability alteration, adhesion, and contact line pinning) play a vital role in immobilizing CO_2. Given the capillary-dominant conditions representative of most reservoir processes (i.e., low capillary number[63]), the trapping is a result of capillary fingering (caused by unfavorable mobility ratio between invading and defending fluids) and snap-off at converging-diverging pore throats. Here, the difference between the 8.5 and 12.0 MPa results may be attributed to density difference ($\Delta\rho \approx 750$ kg/m^3 at 8.5 MPa to $\Delta\rho \approx 376$ kg/m^3 at 12 MPa[64,65]), viscosity ratio ($M \approx 37$ at 8.5 MPa to $M \approx 17$ at 12 MPa[63,64]), wettability alteration, CO_2 adhesion, and contact line pinning acting in synergy. This conclusion is consistent with previous work[66,67] that decreased viscosity ratio and density contrast resulted in greater NWP trapping. Compared to the 8.5 MPa case, CO_2 becomes more viscous and less buoyant at 12 MPa which facilitates its immobilization and entrapment.

An effect of $scCO_2$ exposure time on its capillary behavior in reservoirs manifested, with $S_{nw,r}$ increasing from 0.29 in the first 12.0 MPa cycle (fresh limestone sand) to 0.44 in the third test cycle (limestone sand aged for about 4 months in $scCO_2$ prior to experiment). This time dependence can be very important, given the very long storage times for $scCO_2$ in reservoirs. The time impact is possibly correlated with the temporal evolution of wettability induced by $scCO_2$, implied by the scaling-calculated contact angle values in Figure 3 and SI Table S4.

DOI: 10.1021/acs.est.5b00826
Environ. Sci. Technol. 2015, 49, 7208−7217

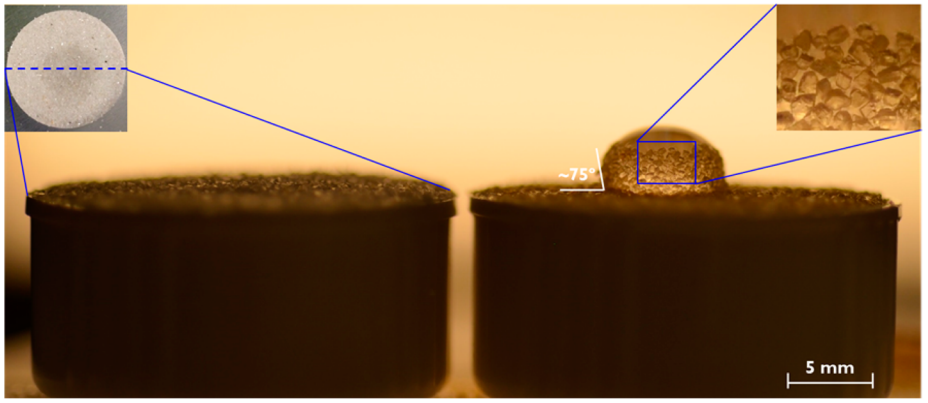

Figure 6. A pre- (left) and post- (right) experiment comparison shows wettability alteration of limestone sands toward more hydrophobic after $scCO_2$ exposure (side view images with DI water droplets added at the surface). The postexperiment sand sample was from the experiment at 12.0 MPa with about 6-month duration of contact with $scCO_2$ in the high pressure chamber. The upper left inset picture is a top view with the darker-colored region being the water spreading area. The upper right inset image shows an enlarged view of the monolayered Pickering type sand coating around the water droplet.

The dependence of $S_{nw,r}$ and C_{trap} on initial NWP saturation $S_{nw,i}$ was examined with data from this study and literature. In Figure 5, data for air−brine, 8.5 and 12.0 MPa $scCO_2$−brine in limestone and quartz sands are presented. The "linear increase−plateau" relation showing increasing $S_{nw,r}$ with increasing $S_{nw,i}$ first, and stabilizing at a maximum level is commonly discussed in the literature.[5,16,22−25,29,43−45] Our results showed the linear increasing trend and are consistent with results from a recent study.[13] A greater $S_{nw,i}$ corresponds to larger CO_2 clusters and ganglia which may more easily connect as a network and thus occupy the pore space more effectively. The local maxima/inflection in the intermediate range of $S_{nw,i}$ as shown in Krevor et al.[28] was not observed. The comparison of results from the $S_{nw,r}$ vs $S_{nw,i}$ experiments and those from the progressive drainage-imbibition experiments suggested the process-dependent behavior reported in a previous work.[13] At similar $S_{nw,i}$, larger equilibration steps (in the $S_{nw,r}$ vs $S_{nw,i}$ experiments) resulted in greater trapping. This may be because of the greater driving force (i.e., greater P_c) that facilitates snap-off.

Time-Dependent Wettability Alteration. Wettability alteration/hysteresis predicted based on results in Figures 2 and 3 is supported by postexperiment observations. All the experiments here started with mostly hydrophilic limestone/dolomite sand (with only a small portion floating on the surface when mixed with excess brine, indicating a minor fraction initially in a more hydrophobic state). After the ETP experiments ended, some sand (mostly desaturated with brine being drained) was immersed in fresh DI water. More sand floated on the water surface relative to the pre-experiment case. With gentle stirring, the $scCO_2$-exposed sand aggregated around air bubbles in the water, forming Pickering type structures.[68] This phenomenon indicates again that the wettability of limestone sand shifted toward more hydrophobic through exposure to $scCO_2$−brine over time.

Further evidence of wettability change was obtained through our direct measurement of wettability on the sand after the ETP experiments. At RTP, air-dried sand previously exposed to $scCO_2$−brine was repacked, and a droplet of DI water was added onto its surface. As shown in Figure 6, the sand was observed to be nearly intermediate wetting after experiment, in contrast to the complete water wetting and spreading before experiment. At the moment that water droplet was added, sand "climbed" around the water droplet and quickly formed a monolayered "sand coat". This observation supports our hypothesis of wettability evolving toward more CO_2 wetting over time. Again, the wettability alteration can be caused by CO_2 adhesion, contact line pinning as well as a stabilized interface reaching hydrophilic/CO_2-phillic balance (HCB) at the presence of colloidal particles/nanoparticles (e.g., Fe_2O_3, Fe_3O_4, and SiO_2).[69]

Regarding the impact of wettability alteration on $S_{nw,r}$ and C_{trap}, reported mechanisms and data appear contradictory. Few comprehensive studies integrating P_c−S_w and wettability alteration information exist, even for oil−water−mineral systems. One group of studies[70−72] showed residual oil saturation decreased with wettability shifting from water wetting to intermediate wetting. Similar results with $scCO_2$-wet media were recently reported by Chaudhary et al.,[47] while $scCO_2$ in more water-wet media has been found to retain hydrophilic capillary behavior.[5,28,30] However, results from a second group of studies[27,32,54] are more consistent with ours on limestone sand, showing greater NWP trapping with wettability shifting toward more intermediate wetting in $scCO_2$−brine systems. The experiments by El-Maghraby and Blunt[54] have particular relevance here, because they were conducted on limestone cores. Thus, the common assumption that S_{nwr,CO_2} can be predicted based on the behavior of other NWPs (e.g., air, oil, and gas)[46,73,74] is not consistently supported by the growing body of experimental evidence. For the first group of studies, the dominant mechanism could be that increased NWP wettability causes less trapping due to a decreased P_c at the CO_2−brine interface which results in less-curved interface, more piston-like displacement and thus decreased snap-off efficiency. For the second group of observations, the controlling mechanism could be that increased NWP wettability causes more trapping due to thinned water film and enhanced CO_2 affinity (possibly adhesion) with minerals.[56,75] The overall trapping behavior results from these two competing mechanisms, and the discrepancy between measured $S_{nw,r}$ and estimated lower $S_{nw,r}$ based on oil and gas may result from differences in pore-scale and perhaps interface-scale dynamics of $scCO_2$ versus oil and gas.

Environmental Implications. This work is important for understanding CO_2 behavior in GCS reservoirs, especially during the postinjection stage where nearly stagnant $scCO_2$

DOI: 10.1021/acs.est.5b00826
Environ. Sci. Technol. 2015, 49, 7208−7217

remains in pores for tens to thousands of years. The P_c–S_w results during the cyclic drainage and imbibition events have relevance for at least three classes of important problems in GCS, namely (1) injection depth, (2) leakage potential, and (3) trapping capacity. The P_c–S_w data provide information useful for injection pressures and the pore pressure threshold (capillary barrier) that should be maintained to prevent CO_2 leakage. The $S_{nw,r}$ and $S_{nw,r}$ vs $S_{nw,i}$ data are valuable for understanding reservoir storage capacities, and suggest that with slightly deeper injection (e.g., 1.2 km compared to 0.85 km) significantly greater trapping is achievable. Compared with quartz-rich reservoirs of similar porosity (8–35% $S_{nw,r}$),[13,29,32] carbonate reservoirs may possess larger trapping capacities. Moreover, reservoir wettability is once again demonstrated to strongly affect the pore displacement processes, and thus the overall fate and transport of CO_2 governed by the force balances between buoyancy force, interfacial tension force, and shear drag force.[76,77] This work also extended the duration of laboratory GCS studies, yielding drainage-imbibition results over months of contact with $scCO_2$–brine to help improve long-term projections of CO_2 storage. Similar investigations on consolidated core samples are needed to better understand the fate of $scCO_2$ in reservoirs.

■ ASSOCIATED CONTENT

Supporting Information

More information about our experimental methods and additional results are provided in the Supporting Information document. The Supporting Information is available free of charge on the ACS Publications website at DOI: 10.1021/acs.est.5b00826.

■ AUTHOR INFORMATION

Corresponding Author

* Phone: 1-510-486-7176; fax: 1-510-486-5686; e-mail: tktokunaga@lbl.gov.

Notes

The authors declare no competing financial interest.

■ ACKNOWLEDGMENTS

This work was carried out under funding support from the Center for Nanoscale Control of Geologic CO_2, (NCGC), an Energy Frontier Research Center (EFRC) funded by the U.S. Department of Energy, Office of Science, Office of Basic Energy Sciences under award DE-AC02-05CH11231. We thank our colleagues Jiamin Wan, Wenming Dong, and Yongman Kim for their great help in method development and data collection. The authors are appreciative of the five anonymous reviewers for their helpful suggestions that lead to improved presentation.

■ REFERENCES

(1) Intergovernmental Panel on Climate Change (IPCC). *Underground Geological Storage, in IPCC Special Report on Carbon Dioxide Capture and Storage*; Cambridge University Press, Cambridge, 2005, 195–276.

(2) Hawkes, C. D.; McLellan, P. J.; Bachu, S. Geomechanical factors affecting geological storage of CO_2 in depleted oil and gas reservoirs. *J. Can. Petrol. Technol.* **2005**, *44*, 52–61.

(3) Qi, R.; LaForce, T. C.; Blunt, M. J. Design of carbon dioxide storage in aquifers. *Int. J. Greenhouse Gas Control* **2009**, 3 (2), 195–205.

(4) Gittins, P.; Iglauer, S.; Pentland, C. H.; Al-Mansoori, S.; Al-Sayari, S.; Bijeljic, B.; Blunt, M. J. Nonwetting phase residual saturation in sand packs. *J. Porous Media* **2010**, *13* (7), 591–599.

(5) Pentland, C. H.; Al-Mansoori, S.; Iglauer, S.; Bijeljic, B.; Blunt, M. J. Measurement of non-wetting phase trapping in sand packs. *Soc. Petrol. Eng. J.* **2010**, *15* (2), 274–281.

(6) Bachu, S.; Bonijoly, D.; Bradshaw, J.; Burruss, R.; Holloway, S.; Christensen, N. P.; Mathiassen, O. M. CO_2 storage capacity estimation: Methods and gaps. *Int. J. Greenhouse Gas Control* **2007**, *1*, 430–443.

(7) Benson, S. M.; Cole, D. R. CO_2 sequestration in deep sedimentary formations. *Elements* **2008**, *4*, 325–331.

(8) Haines, W. B. Studies in the physical properties of soil: V. The hysteresis effect in capillary properties, and the modes of moisture distribution associated therewith. *J. Agric. Sci.* **1930**, *20*, 97–116.

(9) Mason, G.; Morrow, N. R. Developments in spontaneous imbibition and possibilities for future work. *J. Pet. Sci. Eng.* **2013**, *110*, 268–293.

(10) Raeesi, B.; Morrow, N. R.; Mason, G. Capillary pressure hysteresis behavior of three sandstones measured with a multistep outflow–inflow apparatus. *Vadose Zone J.* **2014**, *13*, 3.

(11) Roof, J. G. Snap-off of oil droplets in water-wet pores. *Soc. Petrol. Eng. J.* **1970**, *10* (01), 85–90.

(12) Berg, S.; Ott, H.; Klapp, S. A.; Schwing, A.; Neiteler, R.; Brussee, N.; Makurata, A.; Leua, L.; Enzmann, F.; Schwarz, J.-O.; Kersten, M.; Irvinec, S.; Stampanoni, M. Real-time 3D imaging of Haines jumps in porous media flow. *Proc. Natl. Acad. Sci. U. S. A.* **2013**, *110* (10), 3755–3759.

(13) Zuo, L.; Benson, S. M. Process-dependent residual trapping of CO_2 in sandstone. *Geophys. Res. Lett.* **2014**, *41* (8), 2820–2826.

(14) Geffen, T. M.; Parrish, D. R.; Haynes, G. W.; Morse, R. A. Efficiency of gas displacement from porous media by liquid flooding. *Trans. Metall. Soc. AIME* **1952**, *195*, 29–38.

(15) Crowell, D. C.; Dean, G. W.; Loomis, A. G. Efficiency of gas displacement from a water-drive reservoir. *Bureau of Mines. Report of Investigations*; United States Bureau of the Interior, 1966, Vol. *6735*.

(16) Land, C. S. Comparison of calculated with experimental imbibition relative permeability. *Soc. Petrol. Eng. J.* **1971**, *11* (04), 419–425.

(17) Ma, T. D.; Youngren, G. K. Performance of immiscible water-alternating-gas (IWAG) injection at Kuparuk River unit north slope Alaska. In *SPE Annual Technical Conference and Exhibition*. 1994, Society of Petroleum Engineers.

(18) Jerauld, G. R. Prudhoe Bay gas/oil relative permeability. *SPE Reservoir Eng.* **1997**, *12* (1), 66–73.

(19) Kleppe, J.; Delaplace, P.; Lenormand, R.; Hamon, G.; Chaput, E. Representation of capillary pressure hysteresis in reservoir simulation. *SPE Annual Technical Conference* **1997**, 597–604.

(20) Kralik, J. G.; Manak, L. J.; Jerauld, G. R.; Spence, A. P. Effect of trapped gas on relative permeability and residual oil saturation in an oil-wet sandstone. In *SPE Annual Technical Conference and Exhibition*; Society of Petroleum Engineers, 2000.

(21) Suzanne, K.; Hamon, G.; Billiotte, J.; Trocme, V. Experimental relationships between residual gas saturation and initial gas saturation in heterogeneous sandstone reservoirs. In *SPE Annual Technical Conference and Exhibition*; Society of Petroleum Engineers, 2003.

(22) Chierici, G. L.; Ciucci, G. M.; Long, G. Experimental research on gas saturation behind the water front in gas reservoirs subjected to water drive. In *6th World Petroleum Congress*; World Petroleum Congress, 1963.

(23) Delclaud, J. Laboratory measurements of the residual gas saturation. In *Second European Core Analysis Symposium*; London, 1991, 431–451.

(24) Al Mansoori, S. K.; Itsekiri, E.; Iglauer, S.; Pentland, C. H.; Bijeljic, B.; Blunt, M. J. Measurements of non-wetting phase trapping applied to carbon dioxide storage. *Int. J. Greenhouse Gas Control* **2010**, *4* (2), 283–288.

DOI: 10.1021/acs.est.5b00826
Environ. Sci. Technol. 2015, 49, 7208–7217

(25) Land, C. S. Calculation of imbibition relative permeability for two- and three-phase flow from rock properties. *Trans. Metall. Soc. AIME* **1968**, *243*, 149−156.
(26) Aissaoui, A. Etude théorique et expérimentale de l'hystérésis des pressions capillaries et des perméabilitiés relatives en vue du stockage souterrain de gaz. PhD thesis Ecole des Mines de Paris, 1983.
(27) Plug, W. J.; Bruining, J. Capillary pressure for the sand−CO_2−water system under various pressure conditions. Application to CO_2 sequestration. *Adv. Water Resour.* **2007**, *30* (11), 2339−2353.
(28) Krevor, S.; Pini, R.; Li, B.; Benson, S. M. Capillary heterogeneity trapping of CO_2 in a sandstone rock at reservoir conditions. *Geophys. Res. Lett.* **2011**, *38*(15).
(29) Pentland, C. H.; El-Maghraby, R.; Iglauer, S.; Blunt, M. J. Measurements of the capillary trapping of super-critical carbon dioxide in Berea sandstone. *Geophys. Res. Lett.* **2011**, *38*(6).
(30) Pini, R.; Krevor, S.; Benson, S. M. Capillary pressure and heterogeneity for the CO_2/water system in sandstone rocks at reservoir conditions. *Adv. Water Resour.* **2012**, *38*, 48−59.
(31) Pini, R.; Benson, S. M. Simultaneous determination of capillary pressure and relative permeability curves from core-flooding experiments with various fluid pairs. *Water Resour. Res.* **2013**, *49* (6), 3516−3530.
(32) Tokunaga, T. K.; Wan, J.; Jung, J. W.; Kim, T. W.; Kim, Y.; Dong, W. Capillary pressure and saturation relations for supercritical CO_2 and brine in sand: High-pressure $P_c(S_w)$ controller/meter measurements and capillary scaling predictions. *Water Resour. Res.* **2013**, *49* (8), 4566−4579.
(33) Leverett, M. C. Capillary behavior in porous solids. *Trans. Metall. Soc. AIME* **1941**, *142*, 152−169.
(34) Rose, W.; Bruce, W. A. Evaluation of capillary character in petroleum reservoir rock. *Trans. Metall. Soc. AIME* **1949**, *186* (5), 127−142.
(35) Miller, E. E.; Miller, R. D. Physical theory for capillary flow phenomena. *J. Appl. Phys.* **1956**, *4*, 324−332.
(36) Klute, A.; Wilkinson, G. E. Some tests of the similar media concept of capillary flow: 1. Reduced capillary conductivity and moisture characteristic data. *Soil Sci. Soc. Am. J.* **1958**, *22*, 278−281.
(37) Schroth, M. H.; Ahearn, S. J.; Selker, J. S.; Istok, J. D. Characterization of Miller-similar silica sands for laboratory hydrologic studies. *Soil Sci. Soc. Am. J.* **1996**, *60*, 1331−1339.
(38) Parker, J. C.; Lenhard, R. J.; Kuppusamy, T. A parametric model for constitutive properties governing multiphase flow in porous media. *Water Resour. Res.* **1987**, *23* (4), 618−624.
(39) Selker, J. S.; Schroth, M. H. Evaluation of hydrodynamic scaling in porous media using finger dimensions. *Water Resour. Res.* **1998**, *34* (8), 1935−1940.
(40) Tokunaga, T. K.; Olson, K. R.; Wan, J. Conditions necessary for capillary hysteresis in porous media: Tests of grain size and surface tension influences. *Water Resour. Res.* **2004**, *40*, WO5111.
(41) Anderson, W. G. Wettability literature survey-part 4: Effects of wettability on capillary pressure. *J. Petrol. Technol.* **1987**, *39* (10), 1283−1300.
(42) Morrow, N. R. Wettability and its effect on oil recovery. *J. Petrol. Technol.* **1990**, *42* (12), 1476−1484.
(43) Krevor, S.; Pini, R.; Zuo, L.; Benson, S. M. Relative permeability and trapping of CO_2 and water in sandstone rocks at reservoir conditions. *Water Resour. Res.* **2012**, *48*, 2.
(44) Akbarabadi, M.; Piri, M. Relative permeability hysteresis and capillary trapping characteristics of supercritical CO_2/brine systems: An experimental study at reservoir conditions. *Adv. Water Resour.* **2013**, *52*, 190−206.
(45) Iglauer, S.; Wulling, W.; Pentland, C. H.; Al-Mansoori, S. K.; Blunt, M. J. Capillary-trapping capacity of sandstones and sandpacks. *Soc. Petrol. Eng. J.* **2011a**, *16* (4), 778−783.
(46) Tanino, Y.; Blunt, M. J. Laboratory investigation of capillary trapping under mixed-wet conditions. *Water Resour. Res.* **2013**, *49* (7), 4311−4319.
(47) Chaudhary, K.; Cardenas, B. M.; Wolfe, W. W.; Maisano, J. A.; Ketcham, R. A.; Bennett, P. C. Pore-scale trapping of supercritical CO_2 and the role of grain wettability and shape. *Geophys. Res. Lett.* **2013**, *40* (15), 3878−3882.
(48) Andrew, M.; Bijeljic, B.; Blunt, M. J. Pore-scale imaging of geological carbon dioxide storage under in situ conditions. *Geophys. Res. Lett.* **2013**, *40* (15), 3915−3918.
(49) Andrew, M.; Bijeljic, B.; Blunt, M. J. Pore-scale imaging of trapped supercritical carbon dioxide in sandstones and carbonates. *Int. J. Greenhouse Gas Control* **2014**, *22*, 1−14.
(50) Tokunaga, T. K.; Shuman, D. A method to control low capillary pressure differences over arbitrarily high total pressures. Lawrence Berkeley National Laboratory, Invention Disclosure 2010, IB-2931.
(51) Kim, Y.; Wan, J.; Kneafsey, T. J.; Tokunaga, T. K. Dewetting of silica surfaces upon reactions with supercritical CO_2 and brine: pore-scale studies in micromodels. *Environ. Sci. Technol.* **2012**, *46* (7), 4228−4235.
(52) van Genuchten, M. T. A closed-form equation for predicting the hydraulic conductivity of unsaturated soils. *Soil Sci. Soc. Am. J.* **1980**, *44* (5), 892−898.
(53) Bull, Ø.; Bratteli, F.; Ringen, J. K.; Melhuus, K.; Bye, A. L.; Iversen, J. E. The quest for the true residual gas saturation−An experimental approach. In *Society of Core Analysts Symposium* 2011, SCA2011−03.
(54) El-Maghraby, R. M.; Blunt, M. J. Residual CO_2 trapping in Indiana limestone. *Environ. Sci. Technol.* **2012**, *47* (1), 227−233.
(55) Senel, O.; Will, R.; Butsch, R. J. Integrated reservoir modeling at the Illinois Basin−Decatur Project. *Greenhouse Gases: Sci. Technol.* **2014**, *4* (5), 662−684.
(56) Wang, S.; Tao, Z.; Persily, S. M.; Clarens, A. F. CO_2 adhesion on hydrated mineral surfaces. *Environ. Sci. Technol.* **2013**, *47* (20), 11858−11865.
(57) Broseta, D.; Tonnet, N.; Shah, V. Are rocks still water-wet in the presence of dense CO_2 or H_2S? *Geofluids* **2012**, *12* (4), 280−294.
(58) Espinoza, D. N.; Santamarina, J. C. Water−CO_2−mineral systems: Interfacial tension, contact angle, and diffusion—Implications to CO_2 geological storage. *Water Resour. Res.* **2010**, *46*(7).
(59) Wang, S.; Edwards, I. M.; Clarens, A. F. Wettability phenomena at the CO_2−brine−mineral interface: implications for geologic carbon sequestration. *Environ. Sci. Technol.* **2012**, *47* (1), 234−241.
(60) Iglauer, S.; Pentland, C. H.; Busch, A. CO_2 wettability of seal and reservoir rocks and the implications for carbon geo-sequestration. *Water Resour. Res.* **2015**, *51*(1).
(61) Gao, L.; McCarthy, T. J. Contact angle hysteresis explained. *Langmuir* **2006**, *22* (14), 6234−6237.
(62) Oldenburg, C. M.; Rinaldi, A. P. Buoyancy effects on upward brine displacement caused by CO_2 injection. *Transp. Porous Media* **2011**, *87* (2), 525−540.
(63) Wang, S.; Clarens, A. F. The effects of CO_2-brine rheology on leakage processes in geologic carbon sequestration. *Water Resour. Res.* **2012**, *48*(8).
(64) National Institute of Standards and Technology (NIST) web-based database: http://webbook.nist.gov/chemistry/fluid/. as of April 2015.
(65) Batzle, M.; Wang, Z. Seismic properties of pore fluids. *Geophysics* **1992**, *57* (11), 1396−1408.
(66) Morrow, N. R.; Chatzis, I.; Taber, J. T. Entrapment and mobilization of residual oil in bead packs. *Soc. Petroleum Eng. Reservoir Eng.* **1988**, *3*, 927−934.
(67) Bennion, B. S.; Bachu, S. Relative permeability characteristics for supercritical CO_2 displacing water in a variety of potential sequestration zones. In *Society of Petroleum Engineers Annual Technical Conference and Exhibition*. **2005**.
(68) Binks, B. P. Particles as surfactants—similarities and differences. *Curr. Opin. Colloid Interface Sci.* **2002**, *7* (1), 21−41.
(69) Worthen, A. J.; Bagaria, H. G.; Chen, Y.; Bryant, S. L.; Huh, C.; Johnston, K. P. Nanoparticle-stabilized carbon dioxide-in-water foams with fine texture. *J. Colloid Interface Sci.* **2013**, *391*, 142−151.
(70) Jadhunandan, P. P.; Morrow, N. R. Effect of wettabiity on waterflood recovery for crude-oil/brine/rock systems. *SPE Reservoir Eng.* **1995**, *10* (1), 40−46.

DOI: 10.1021/acs.est.5b00826
Environ. Sci. Technol. 2015, 49, 7208−7217

(71) Valvatne, P. H.; Blunt, M. J. Predictive pore-scale modeling of two-phase flow in mixed wet media. *Water Resour. Res.* **2004**, *40*(7).
(72) Spiteri, E. J.; Juanes, R.; Blunt, M. J.; Orr, F. M. A new model of trapping and relative permeability hysteresis for all wettability characteristics. *Soc. Petroleum Eng. J.* **2008**, *13* (03), 277−288.
(73) Pentland, C. H.; Al-Mansoori, S.; Iglauer, S.; Bijeljic, B.; Blunt, M. J. Measurement of non-wetting phase trapping in sand packs. In *Society of Petroleum Engineers Annual Technical Conference and Exhibition*; SPE 115697: Denver, CO, 2008.
(74) Iglauer, S.; Paluszny, A.; Pentland, C. H.;Blunt, M. J. Residual CO_2 imaged with X-ray micro-tomography. *Geophys. Res. Lett.* **2011**, *38*(21).
(75) Wan, J.; Kim, Y.; Tokunaga, T. K. Contact angle measurement ambiguity in supercritical CO_2−water−mineral systems: Mica as an example. *Int. J. Greenhouse Gas Control* **2014**, *31*, 128−137.
(76) Corapcioglu, M. Y.; Cihan, A.; Drazenovic, M. Rise velocity of an air bubble in porous media: Theoretical studies. *Water Resour. Res.* **2004**, *40* (4).
(77) Wang, S.; Clarens, A. F. Improved force balance for predicting vertical migration of CO_2 from geologic sequestration sites. In *Carbon Management Technology Conference*, Pittsburgh, 2012.

DOI: 10.1021/acs.est.5b00826
Environ. Sci. Technol. 2015, 49, 7208−7217